UNIVERSITY OF BIRMINGHAM

Description of bow-tie nanoantennas excited by localized emitters using conformal transformation

Pacheco-Pena, Victor; Beruete, Miguel; Fernández-Domínguez, Antonio I; Luo, Yu; Navarro-Cia, Miguel

Document Version
Peer reviewed version

[Link to publication on Research at Birmingham portal](#)

Supporting information: Description of bow-tie nanoantennas excited by localized emitters using conformal transformation

Víctor Pacheco-Peña[†,ξ], Miguel Beruete[†,§], Antonio I. Fernández-Domínguez[‡], Yu Luo[χ], Miguel Navarro-Cía[* Ω,ξ]

[†] Antennas Group – TERALAB, Universidad Pública de Navarra, 31006 Pamplona, Spain

[ξ] Optical and Semiconductor Devices Group, Imperial College London, London SW7 2AZ, UK

[§] Institute of Smart Cities, Public University of Navarra, 31006 Pamplona, Spain

[‡] Departamento de Física Teórica de la Materia Condensada and Condensed Matter Physics Center (IFIMAC), Universidad Autónoma de Madrid, Madrid 28049, Spain

[χ] The Photonics Institute and Centre for OptoElectronics and Biophotonics, School of Electrical & Electronic Engineering, Nanyang Technological University, Singapore 639798, Singapore

[Ω] School of Physics and Astronomy, University of Birmingham, Birmingham B15 2TT, UK

m.navarro-cia@bham.ac.uk; Phone: +44(0)1214144664; Fax: +44(0)1214144644

Resonant condition and discrete distribution of the LSP modes

Let us here study the influence of the angle θ' to the LSP modes and their distribution in the spectra. The LSP modes for the gap bow-tie nanoantennas are distributed at discrete wavelengths following the resonant condition:

$$\left\{(\varepsilon-1)^2\left[e^{k(3d_1+6d_2+2d_3)}-e^{k(d_1+4d_2+4d_3)}\right]-(\varepsilon+1)^2\left[e^{k(d_1+4d_2+2d_3)}-e^{k(3d_1+6d_2+4d_3)}\right]\right\}^2-\left\{2(\varepsilon^2-1)\left[e^{k(3d_1+6d_2+3d_3)}-e^{k(d_1+4d_2+3d_3)}\right]\right\}^2=0 \qquad (1.1)$$

where ε is the permittivity of the metal and k is the wavenumber of the transverse LSP modes calculated as $k=(n\pi-\Delta\varphi)/(L_1+L_2)$ with $n = 1,2,3...$ representing the number of each LSP mode . This resonant condition has been derived from the formulation shown in the Methods section, and taking the condition of divergence of the coefficient of the scattered potential ($B_\pm$). By using this resonant condition, the number of LSP modes supported by the bow-tie nanoantenna under study with total length $l' = 20$ nm as a function of the angle θ' is shown in Figure S1a when a vertical and horizontal dipole is used to illuminate the nanoantenna. The larger θ' is, the lower the number of LSP modes exist. This is due to the LSP modes are directly related to θ (i.e., d_3) when the dimensions L_1 and L_2 are fixed (see eq 1.1). The distribution of the first 15 LSP modes in the spectrum for three specific bow-tie nanoantennas with angles 5º, 25º and 45º is shown Figure S1b,c for a vertically and horizontally polarized dipole, respectively. It can be observed that each resonance of the SP modes is red-shifted when the angle of the antenna is decreased for both polarizations, which is in good agreement with Figure 2. Moreover, it is shown that the higher-order SP modes are compressed when their resonances approaches to the surface plasmon wavelength (λ_{sp}, plotted as a black dotted line).
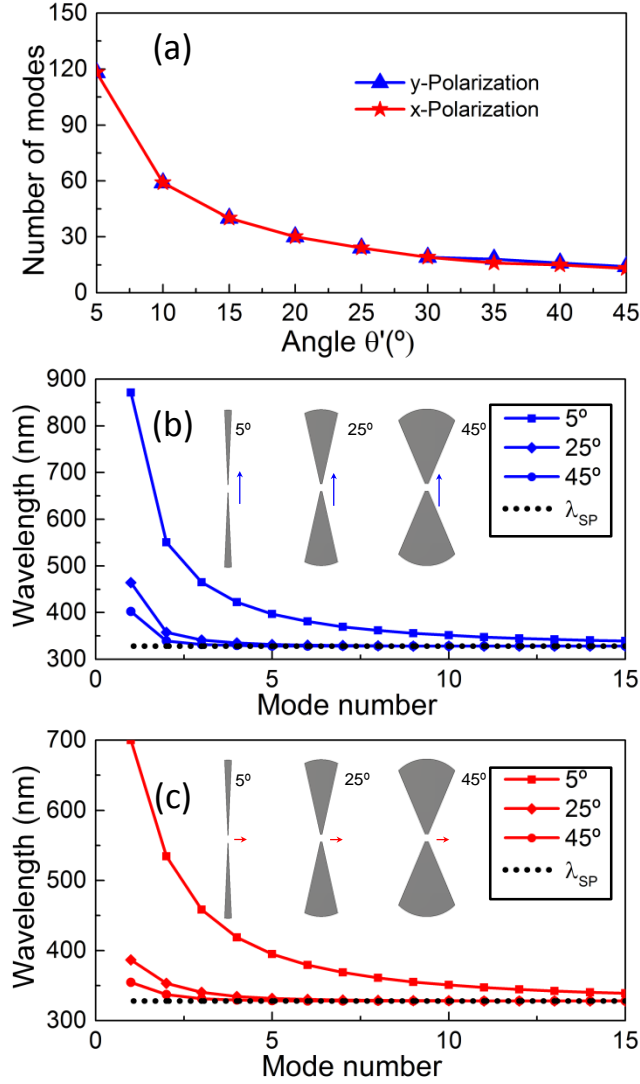
Figure S1. (a) Number of modes as a function of θ' for a dipole illuminating the bow-tie with vertical (blue) and horizontal (red) polarization. Analytical cut-off wavelength for each mode number for bow-tie angle 5° (squares), 25° (diamonds) and 45° (circles) when the illuminating dipole is vertically (b) and horizontally polarized (c) as shown in the insets. The discrete points in (b,c) have been connected with a solid line to guide the eye.

Non-radiative and radiative enhancements along with the absorption cross section.

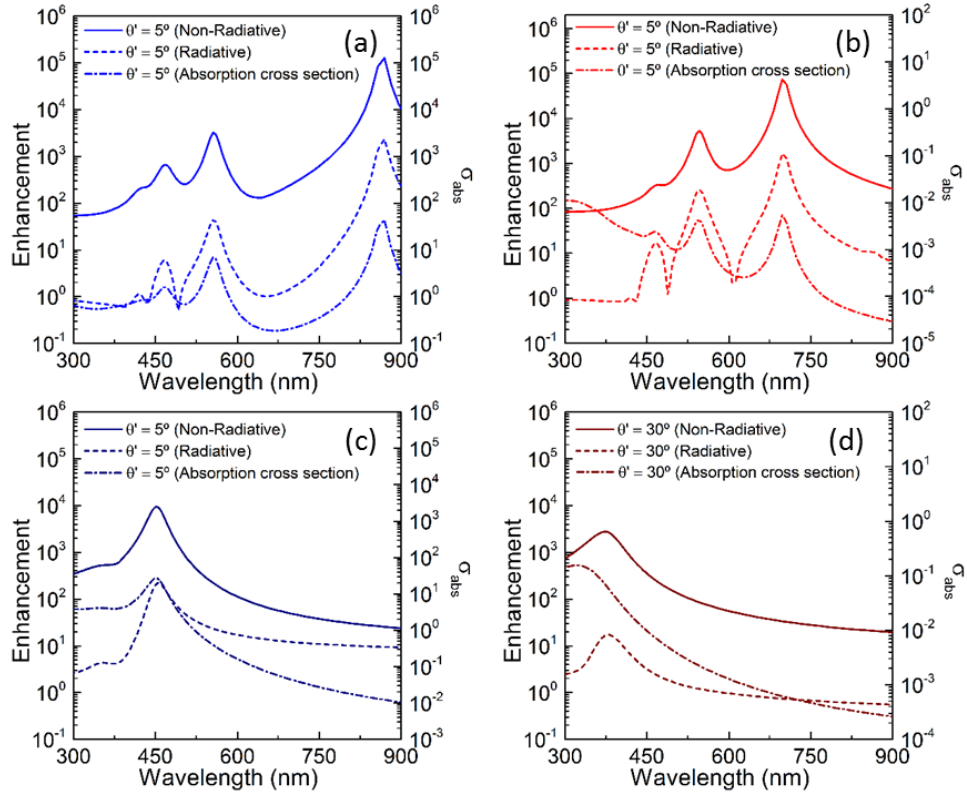**Figure S2.** Simulation results of the non-radiative (continuous lines) and radiative Purcell enhancement (dotted lines) along with the absorption cross section (dashed-dotted lines) for two bow-tie nanoantennas with $\theta' = 5°$ (first row) and $\theta' = 30°$ (second row) when a vertically and a horizontally polarized dipole/plane-wave is used a source, first and second columns respectively.

Spatial absorption distribution for the bow-tie with $\theta' = 30°$.

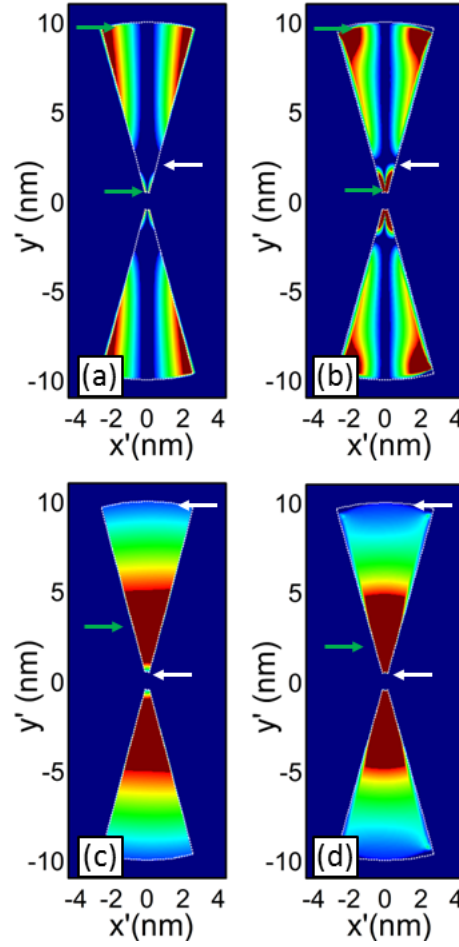**Figure S3.** Analytical (a,c) and simulation-computed (b,d) absorption at the $\Gamma_{nr}(\omega)/\Gamma_0(\omega)$ fundamental peak of the bow-tie with $\theta' = 30°$ when the illuminating dipole is vertical (top) and horizontal (bottom). The color scale bar is saturated to appreciate the details. Horizontal green and white arrows indicate respectively the location of the maxima and minima on the top arm of each bow-tie.

Standing wave pattern in the transformed frame.

In the multi-slab geometry, for a vertically polarized dipole, the field distribution for the $n = 1$ LSP mode has a field distribution with anti-nodes at both extremes of the slab (L_1 and $-L_2$) and a node at the center (in the analogy of a string, this corresponds to the fundamental resonance of the standing wave pattern). Similarly, the $n = 2$ LSP mode has two electric field nodes and three anti-nodes, located at the extremes of the slab and at the center in-between the nodes. On the other hand, for a horizontal emitter, the $n = 1$ LSP mode has a field distribution with nodes at both extremes of the slab and an anti-node at the center; while for the $n = 2$ LSP mode, the field distribution has three nodes (at the center and at both extremes of the slab) and two anti-nodes.

Changing the gap of the bow-tie nanoantenna with $\theta' = 30°$

The $\overline{\Gamma_{nr}}$ peak due to the $n = 1$ LSP mode for the case $\theta' = 30°$ (see Figure S4) has a higher non-radiative Purcell enhancement within the entire range of normalized gaps. The second $\overline{\Gamma_{nr}}$ peak is observed as a shoulder for a vertical dipole (see first column of Figure S4) while it falls beyond the spectral window here evaluated under horizontal illumination (see second column of Figure S4). For this nanoantenna, the $\overline{\Gamma_{nr}}$ peak due to the $n = 1$ LSP mode is also blue-shifted from ~555 nm to ~444 nm (vertical) and from ~382 nm to ~370 nm (horizontal), when the gap is varied between $0.01l'$ and $0.06l'$. Note that, again, for a vertical dipole (see Figure S4a,c) the $\overline{\Gamma_{nr}}$ linked to the first LSP mode vanishes for certain gap sizes, such as $0.01l'$, while such behavior is not observed in the absorption cross section. This underlines the key role played by the position and orientation of the localized emitter. For this bow-tie nanoantenna, the analytical $\overline{\Gamma_{nr}}$ peak due to the $n = 2$ LSP mode is slightly blue-shifted with an average value of 2.9% when a vertical dipole illuminates the bow-tie nanoantennas while, as it has been described, this higher order LSP mode is not observed under a horizontal illumination. Finally, for the sake of completeness, the numerical results of $\overline{\Gamma_r}$ are shown in the third row of Figure S4. Not surprisingly, the dipolar $n = 1$ LSP mode for both dipole polarizations shows higher radiative decay rate than higher-order modes, but still is negligible compared to $\overline{\Gamma_{nr}}$.
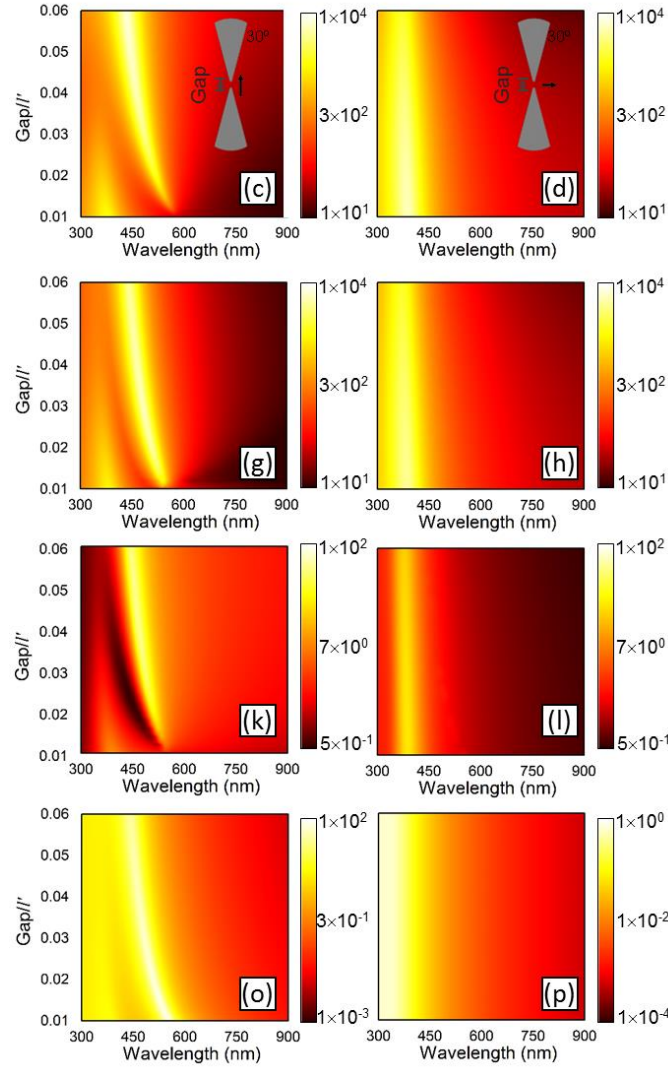
Figure S4. Analytical (first row) and simulated (second row) non-radiative Purcell enhancement spectra along with the simulation results of the radiative Purcell enhancement spectra (third row) and absorption cross section as a function of the gap between the arms for the bow-tie with $\theta' = 30°$ when a vertically (first column) and horizontally (second column) polarized dipole (top three rows) or plane-wave is used as a source (bottom row).

Three-arm bow-tie nanoantenna

Figure S5a shows the scenario comprising a line dipole (nanoemitter) with arbitrary orientation and a tripod nanoantenna made of silver (Ag). By applying the same conformal transformation as in the main text, i.e., $z = \ln(z')$, the tripod nanoantenna is transformed into the multi-slab geometry shown in Figure S5b. Notice that now there are three silver slabs per period, rather than two as for the bow-tie nanoantenna. Following exactly the same methodology as for the bow-tie nanoantenna, the electromagnetic response of this new transformed space can be obtained, and thus, also all spectral feature of the tripod nanoantenna.

As an illustration of the tripod nanoantenna, the results of two different cases are reported here: horizontal and vertical dipole illumination for l'=20 nm, a normalized gap between arms of $0.05l'$ and $\theta' = 30°$. As one could expect based on trigonometric reasoning, the Purcell enhancement spectra shows for both cases two modes associated each one to the $n = 1$ LSP mode of each polarization in the bow-tie nanoantenna. The mode associated to the vertical polarization of the bow-tie nanoantenna emerges ~470 nm, wherehas the mode linked to the horizontal polarization of the bow-tie nanoantenna appears ~ 360 nm. Notice that the non-radiative Purcell enhancement is higher for both cases than for the bow-tie nanoantenna partially because of the larger amount of metal per period. The radiative component is still consistently at least two orders of magnitude smaller than the non-radiative one, and thus negligible, as in the main text for the bow-tie nanoantenna.
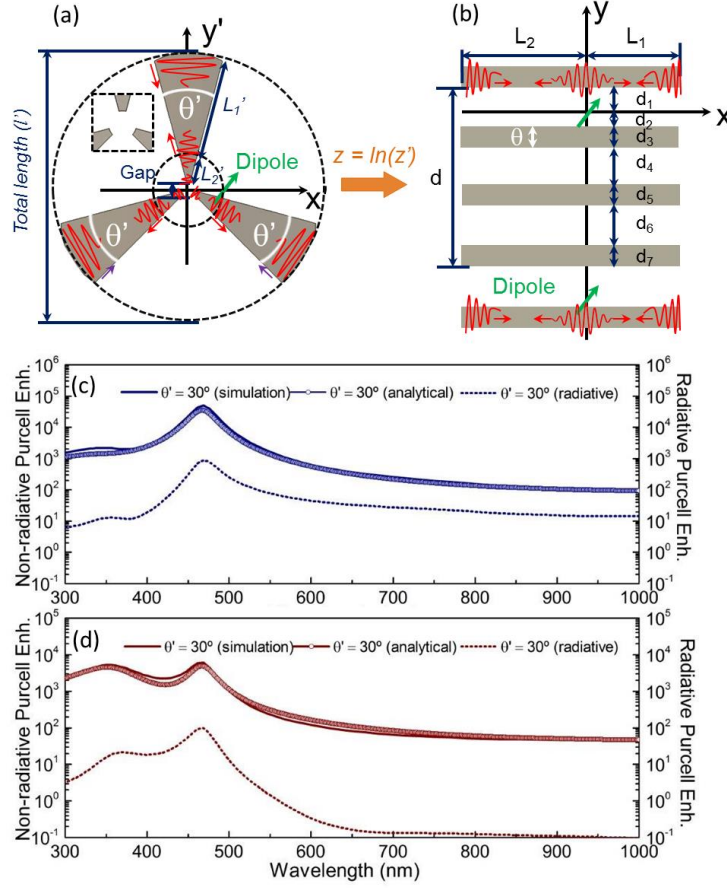
Figure S5. (a) Schematic representation of a metallic tripod with a gap on its center illuminated with a dipole at $(x', y') = (1 \text{ nm}, 0)$ (green arrow). (b) Transformed geometry after the conformal mapping is applied to the tripod. (c, d) Analytical (dots) and numerical (solid lines) results of the non-radiative Purcell enhancement spectra along with the numerical results of the radiative Purcell enhancement (dashed lines) for a tripod nanoantenna made of silver with $\theta' = 30°$ when a vertical (c) and horizontal (d) dipole is used as the radiative source.